

Multi-Spectroscopic Investigations for Comprehensive Structural Analysis of Aluminoborosilicate Glasses: I. Integrating Raman, XPS, XAS and NMR Techniques

(Supplementary materials)

Hanyu Hu¹  <https://orcid.org/0009-0001-4961-3954>, Sami Soudani^{1,2}  <https://orcid.org/0009-0001-9301-2566>,
Jonathan Hamon¹, Nicolas Trcera³  <https://orcid.org/0000-0002-9364-1039>, Michael Paris¹ 
<https://orcid.org/0000-0002-8671-0630>, and Yann Morizet^{1,2}  <https://orcid.org/0000-0001-9599-245X>

¹ Nantes Université, CNRS, Institut des Matériaux Jean Rouxel (IMN), 44322 Nantes Cedex, France

² Nantes Université, Nantes Atlantique Universités, Laboratoire de Planétologie et Géosciences de Nantes (LPG), UMR CNRS 6112, 44322 Nantes Cedex, France

³ Synchrotron SOLEIL, L'Orme des Merisiers, Départementale 128, 91190 Saint-Aubin, France

*Correspondence: Yann Morizet, yann.morizet@univ-nantes.fr

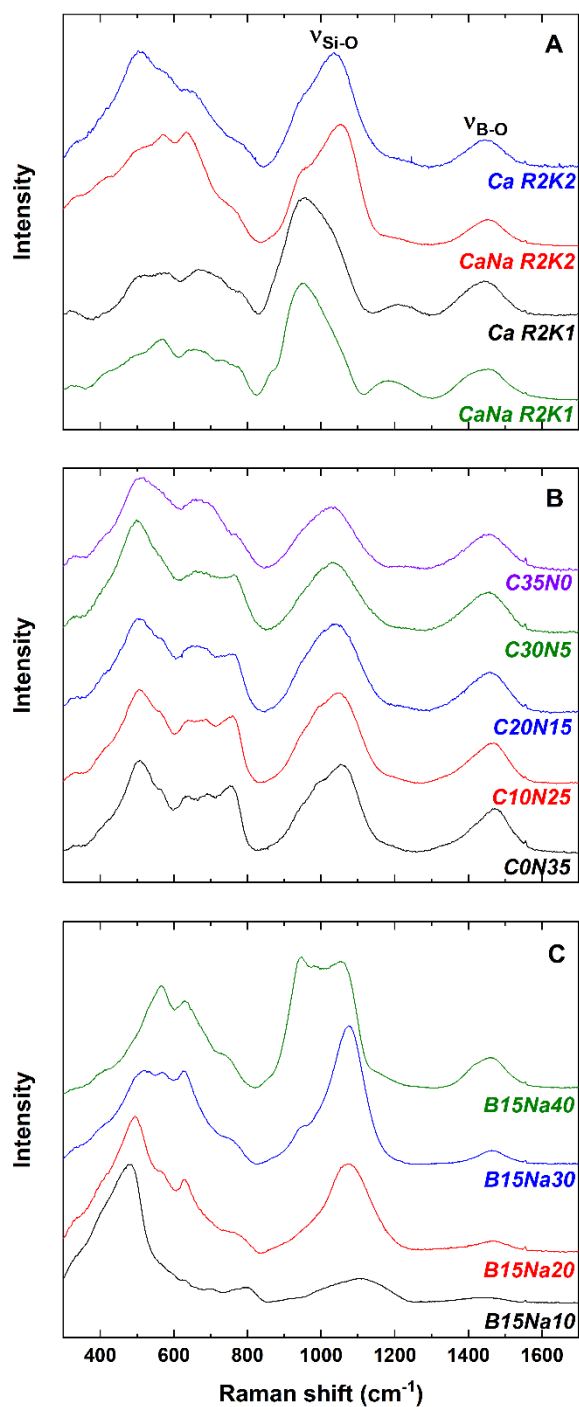


Figure S1. Raman spectra of the CaNa-RnKp, Ca-RnKp (A), CxNy (B) and B15Nay (C) series. The spectra were normalized to the highest intensity after baseline correction between the 300 – 1700 cm^{-1} area.

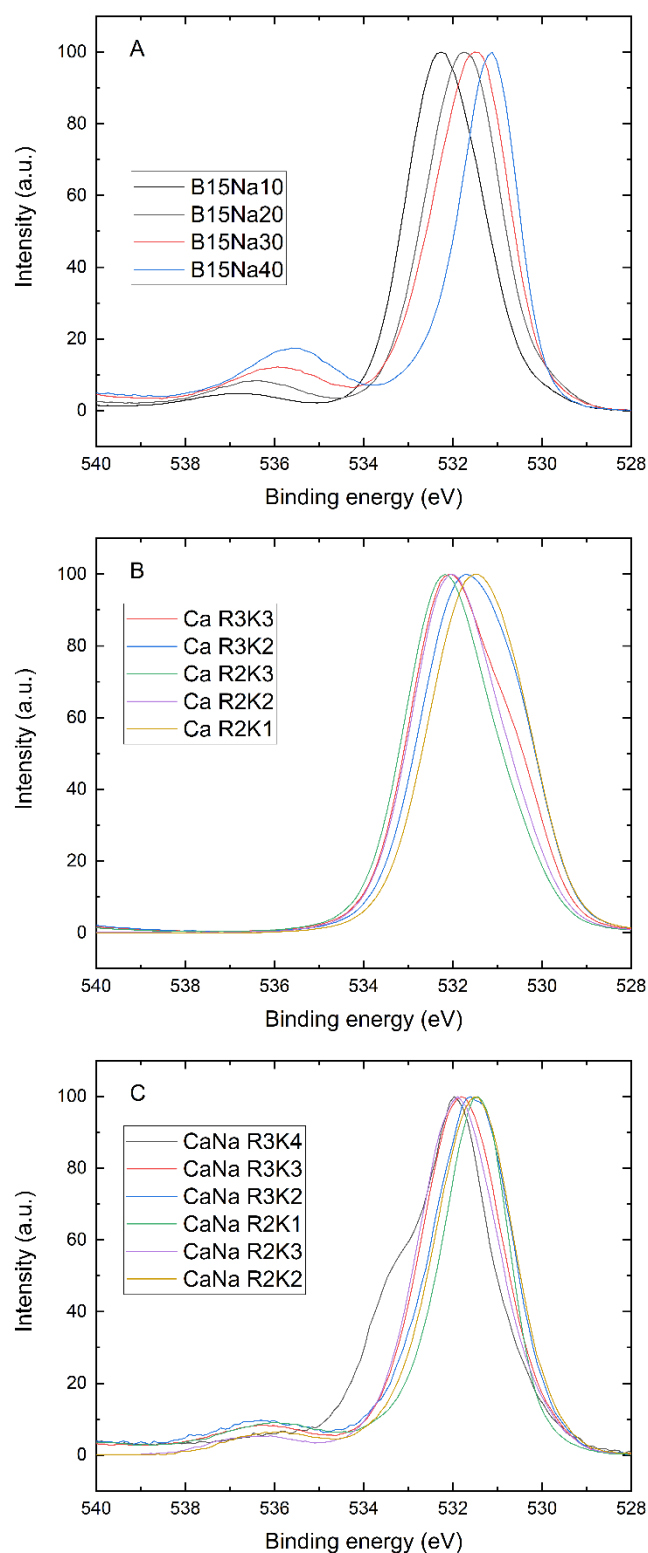


Figure S2. XPS spectra of the B15Nay (A), Ca-RnKp (B) and CaNa-RnKp (C) series. The spectra were normalized to the highest intensity after baseline correction between the 540 – 528 eV area.

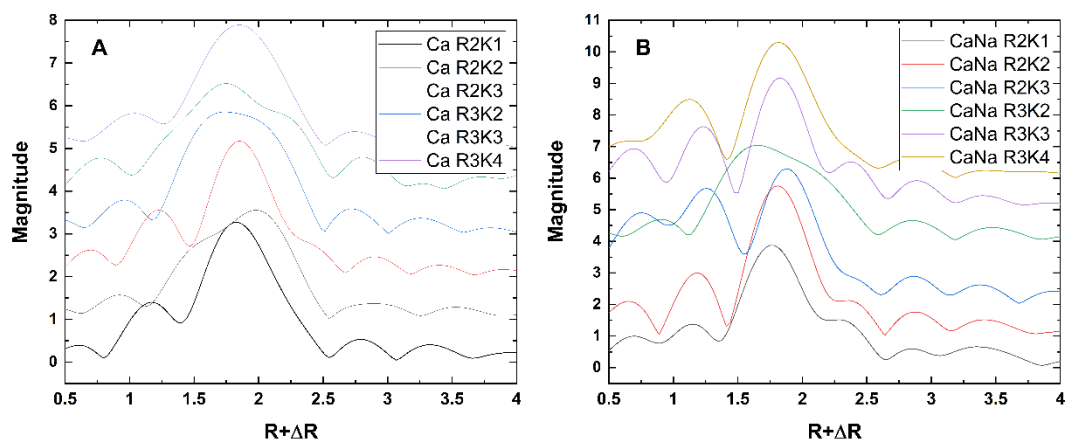


Figure S3. K-edge FT-EXAFS spectra in R-space of the Ca-RnKp (A) and CaNa-RnKp (B) series.

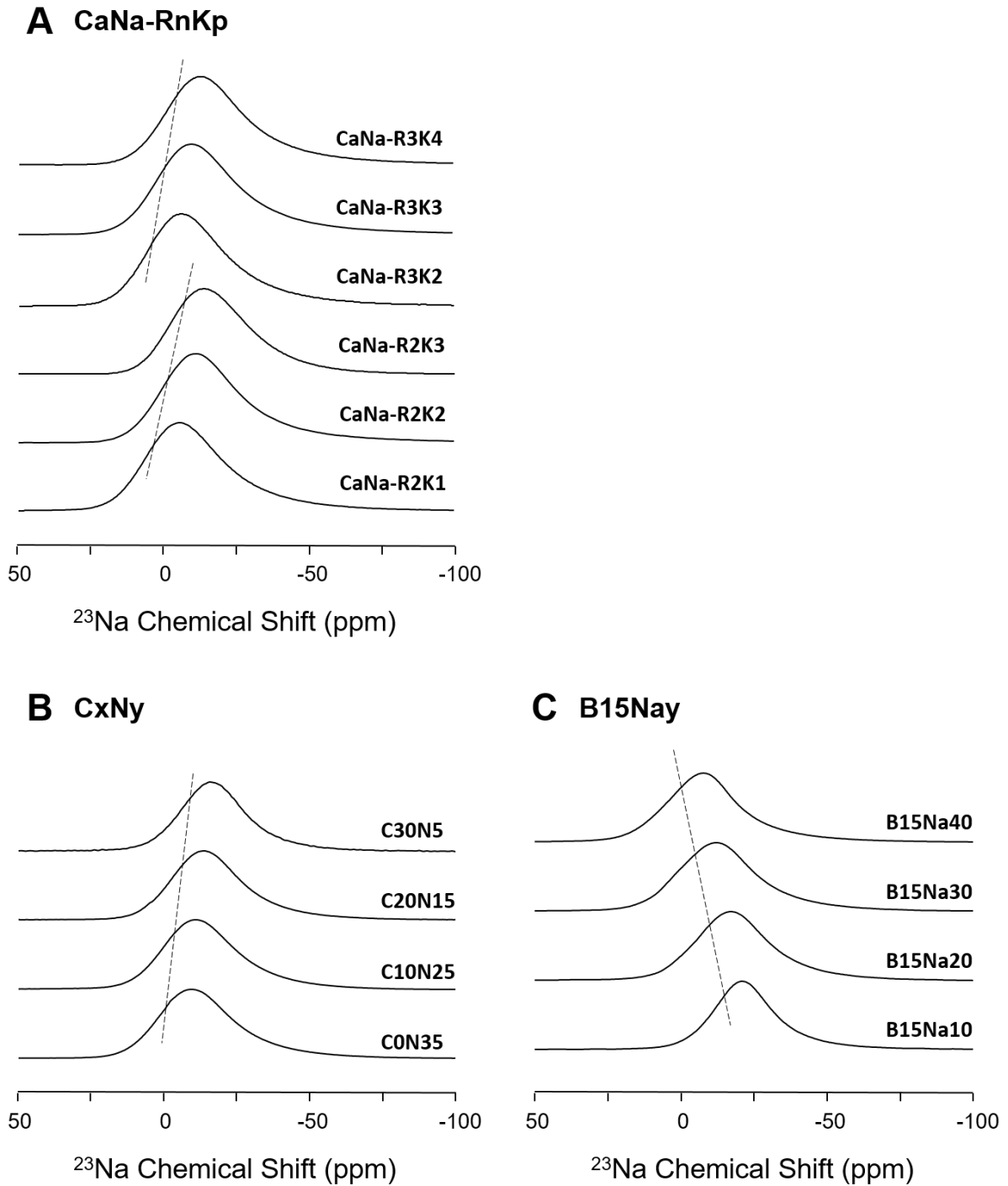


Figure S4. ^{23}Na NMR spectra of CaNa-RnKp (A), CxNy (B) and B15Nay (C) glass series (dashed line indicate the evolution of ^{23}Na isotropic chemical shift. The spectra were normalized to the highest intensity after baseline correction between the 50 - -100 ppm.

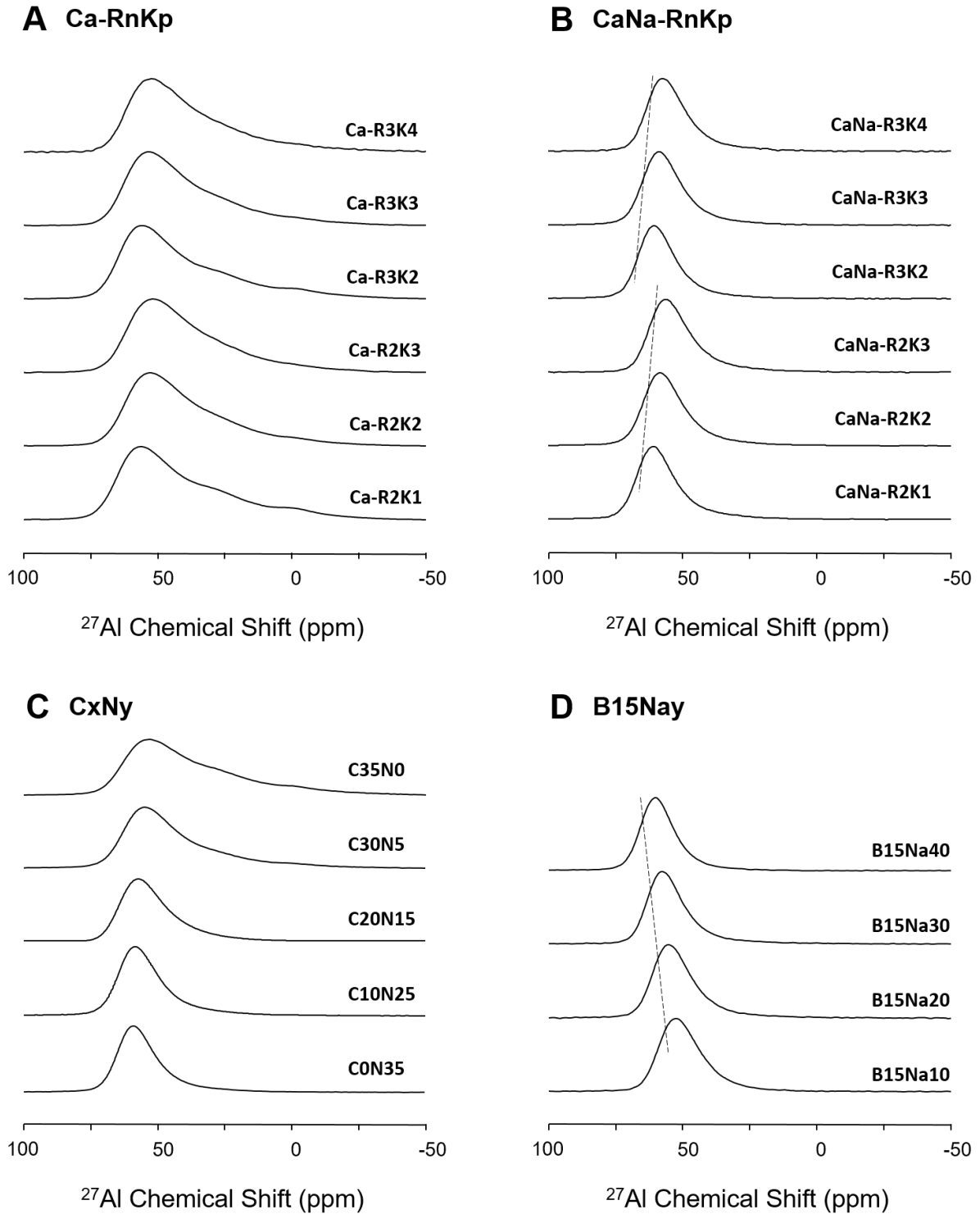


Figure S5. ^{27}Al NMR spectra of Ca-RnKp (A), CaNa-RnKp (B), CxNy (C) and B15Nay (D) glass series (dashed line indicate the evolution of ^{27}Al isotropic chemical shift. The spectra were normalized to the highest intensity after baseline correction between the 100 - -50 ppm).

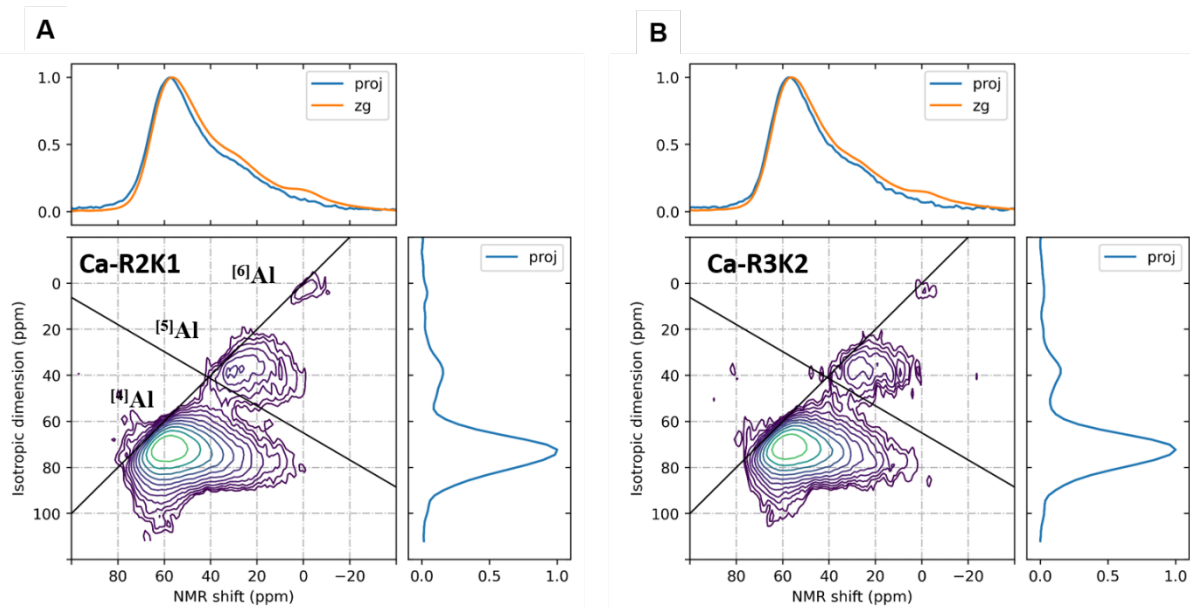


Figure. S6. ^{27}Al 3Q-MAS spectra of Ca-R2K1 (A) and Ca-R3K2 (B), including its MAS projection (top of the map, blue), 1D MAS spectrum (top of the map, orange) and isotropic projection (right of the map). $^{[5]}\text{Al}$ and $^{[6]}\text{Al}$ species are separated in the spectra.

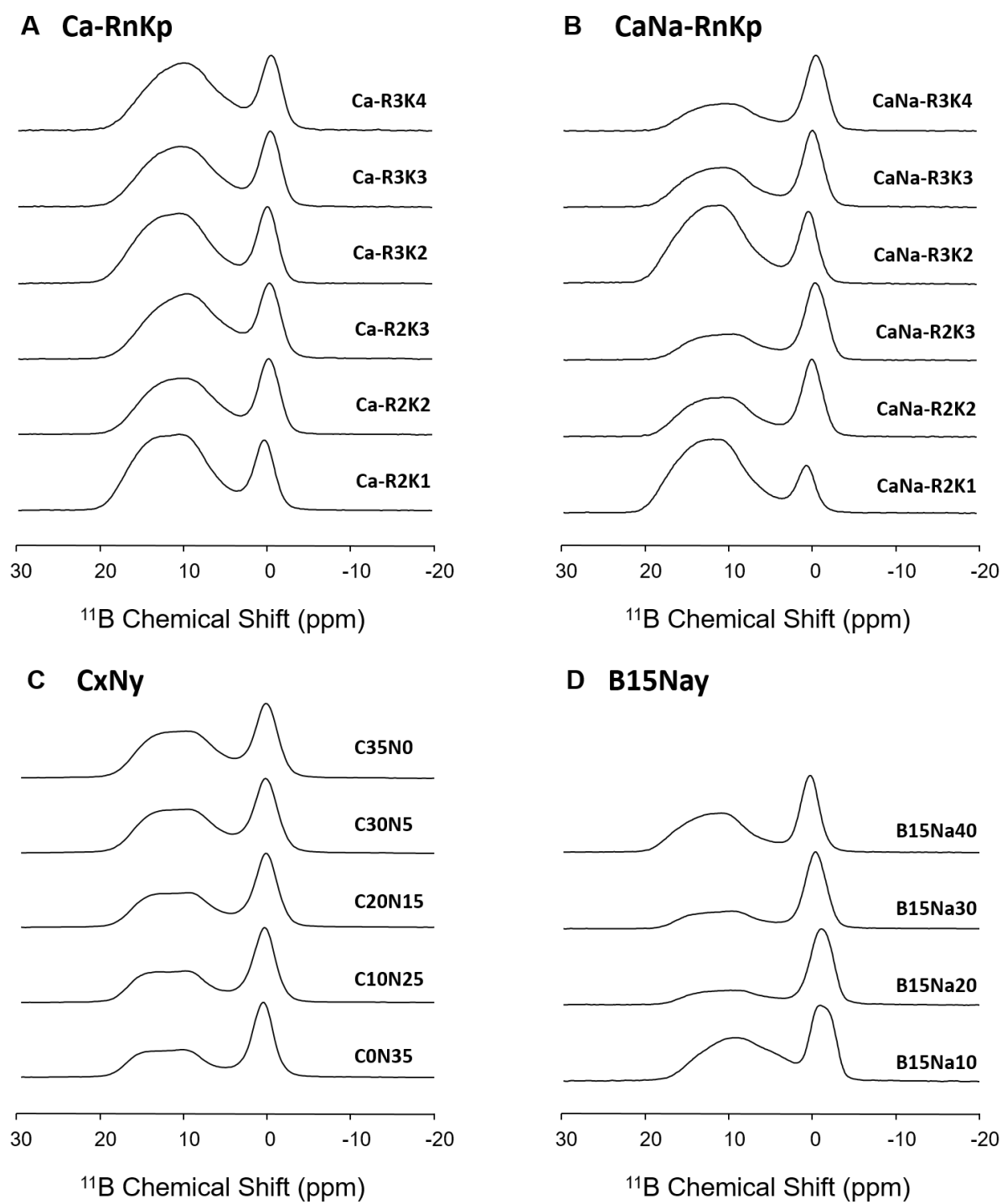


Figure S7. ^{11}B NMR spectra of Ca-RnKp (a), CaNa-RnKp (b), CxNy (c) and B15Nay (d) glass. The spectra were normalized to the highest intensity after baseline correction between the 30 - -20 ppm.

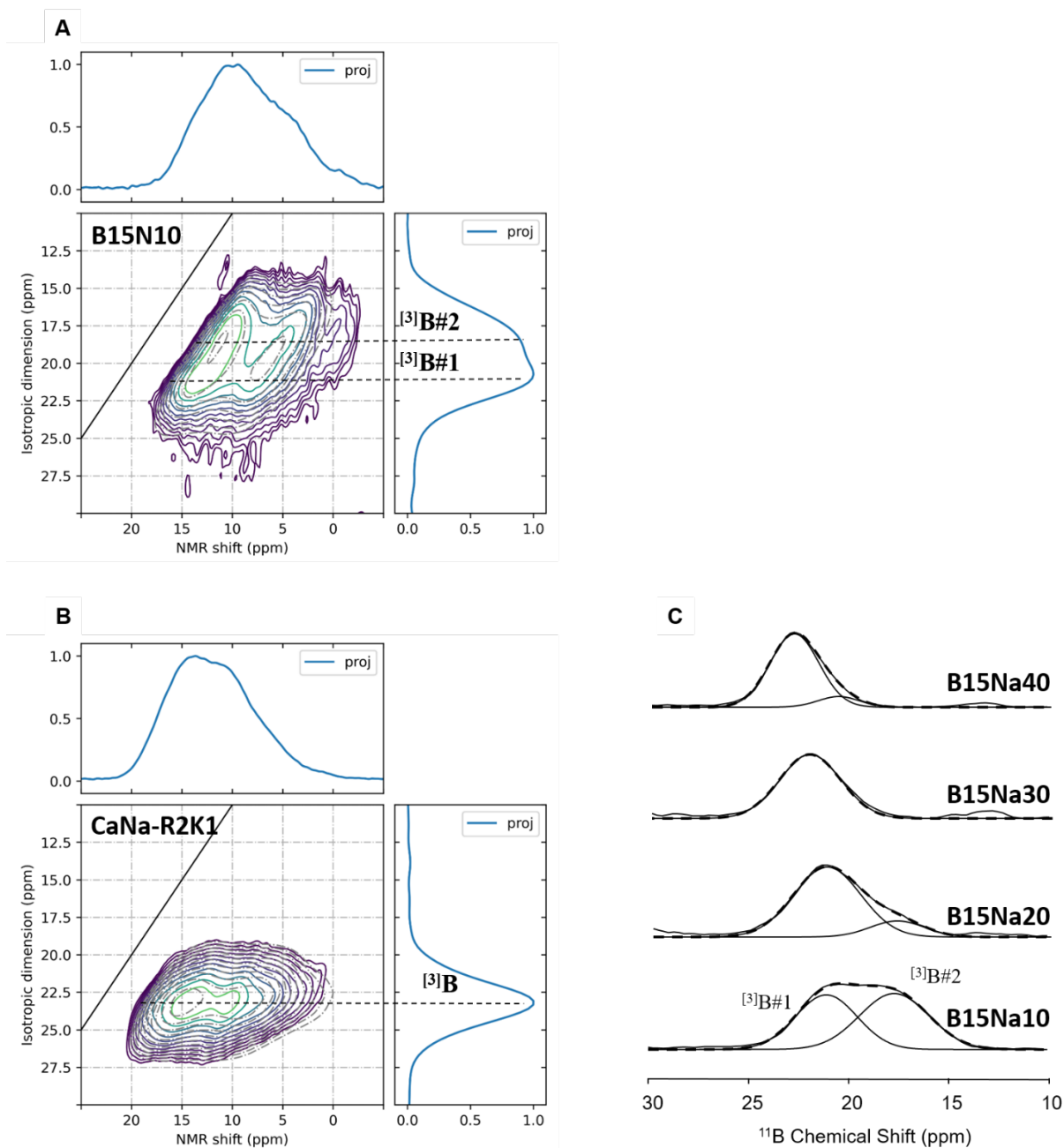


Figure S8. ^{11}B 3Q-MAS ($^{[3]}\text{B}$ part) spectra of B15N10 (A) and CaNa-R2K1 (B), including its fits (green dashed lines), MAS projection (top of the map), and isotropic projection (right of the map), and isotropic projections of ^{11}B 3Q-MAS ($^{[3]}\text{B}$ part) maps of B15Nay glass series (C), (dashed lines represent the decomposition spectra of $^{[3]}\text{B}\#1$ and $^{[3]}\text{B}\#2$ species using Gaussian peaks).

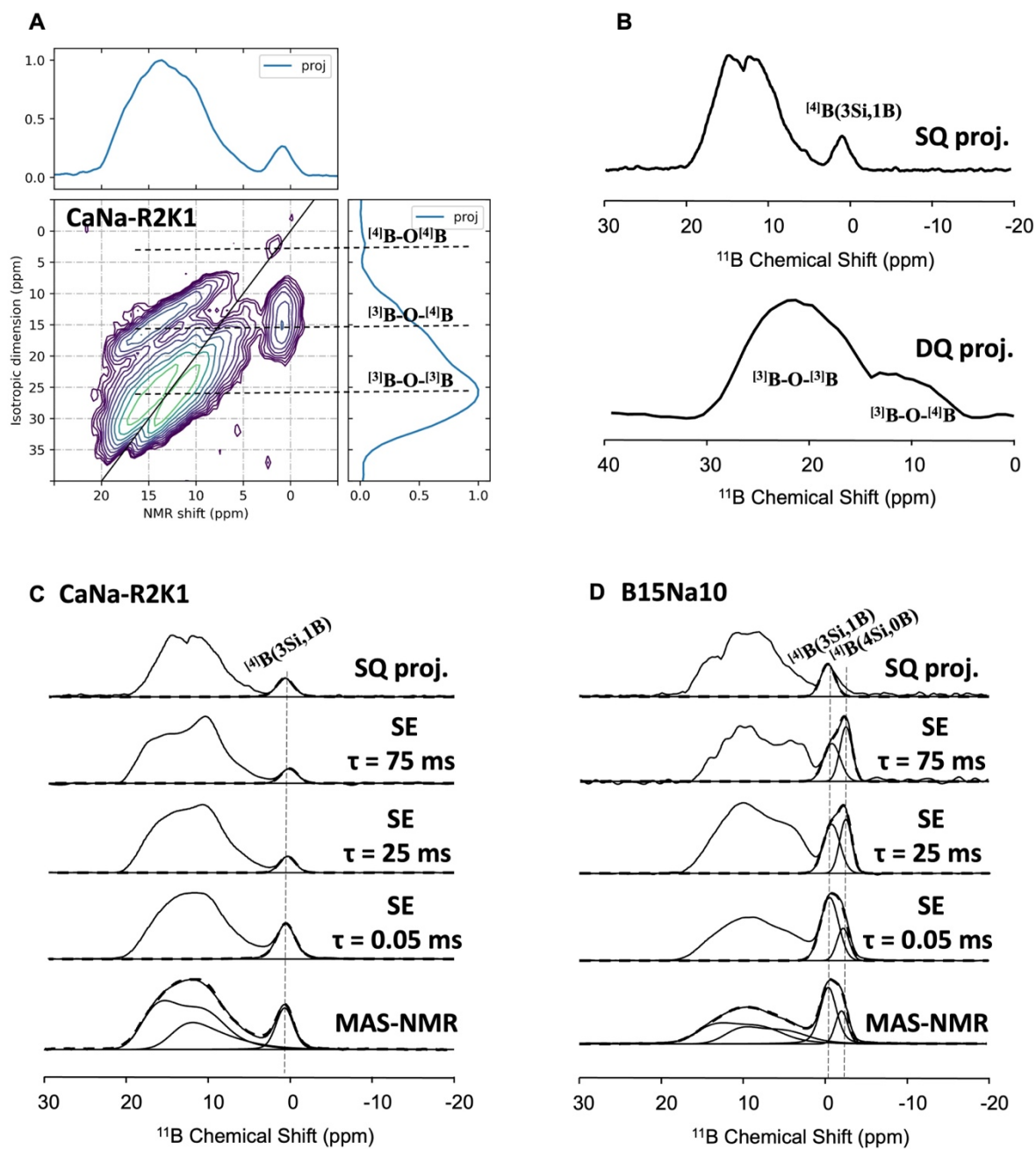


Figure S9. (A) ^{11}B DQ-SQ spectrum of CaNa-R2K1 glass, including the SQ projection (top of the map) and the DQ projection (right of the map). (B) Demonstration of use of SQ and DQ projections. (C) and (D) Examples of ^{11}B NMR spectra curve fitting process: SQ projection of DQ-SQ maps, SE spectra with different echo times and ^{11}B MAS-NMR spectra of B15Na10 (C) and CaNa-R2K1 (D) glasses (dashed lines represent the decomposition spectra using Amorphous model for $^{[3]}\text{B}$ species and Gaussian peaks for $^{[4]}\text{B}$ species).

Table S1. Previous Raman spectroscopic studies of (boro)silicate glasses and melts.

Literature	Frequency (cm ⁻¹)				^[3] B-O- ^[4] B	^[3] B-O- ^[3] B
	Q ¹	Q ²	Q ³	Q ⁴		
B. O. Mysen et al., 1980 [1]	900-920	950-980	1050-1100	1060, 1190		
B. O. Mysen et al., 1982 [2]	900	950	1100	1150, 1200		
D. W. Matson et al., 1983 [3]		950	1100			
P. McMillan, 1984 [4]	900	950-1000	1050-1100	1060, 1200		
J. D. Frantz et al., 1995 [5]		800-900	1050	1100		
R. Akagi et al., 2001 [6]					1380	1490
L. Cormier et al., 2006 [7]					1410	1500
V.P. Zakaznova-Herzog et al., 2007 [8]		930-1090	1100	1100-1150		
M. Lenoir et al., 2008 [9]		900-950	1050-1100	1100-1200	1410	1490
D. Manara et al., 2009 [10]	900-920	950-980	1050-1100	1120-1190	1410	1480
F. Angeli et al., 2012 [11]	900	950	1050	1150		
D. R. Neuville et al., 2014 [12]	950	1050	1100	1150-1200	1410	1490
C. Le Losq et al., 2014 [13]		960	1090	1140, 1170		
B. J.A. Moulton et al., 2021 [14]	850	940	1070			
H.W. Nesbitt et al., 2021 [15]	860	950	1000-1100			

Table S2. Fit parameters deduced from Raman spectra: frequency (**Freq.**, $\pm 10 \text{ cm}^{-1}$), full width at half maximum (**w.**, $\pm 10 \text{ cm}^{-1}$) of frequency distribution and proportion of peak area (**%A**, $\pm 3 \%$).

Glass ID	Raman spectra (silicate region) deconvolution										Raman spectra (borate region) deconvolution			
	S1		S2		S3		S4		S5		B1		B2	
	Freq./w. (cm^{-1})	%A (%)	Freq./w. (cm^{-1})	%A (%)	Freq./w. (cm^{-1})	%A (%)	Freq./w. (cm^{-1})	%A (%)	Freq./w. (cm^{-1})	%A (%)	Freq./w. (cm^{-1})	%A (%)	Freq./w. (cm^{-1})	%A (%)
CaNa-RnKp														
CaNa-R2K1	857.9/28.3	2.9	932.1/66.5	43.9	983.8/56.0	30.7	1038.3/64.2	21.9	1190.7/79.9	9.0	1404.7/79.7	44.8	1473.0/83.6	55.2
CaNa-R2K2	856.8/45.4	0.7	947.6/70.0	27.5	1017.2/67.8	43.9	1073.1/69.2	38.8	1181.2/73.4	2.9	1415.2/73.3	39.5	1469.5/73.2	60.5
CaNa-R2K3	868.1/70.2	1.4	954.1/72.2	18.3	1035.5/72.2	43.2	1091.0/70.1	39.2	1171.0/62.1	4.6	1419.9/81.5	42.3	1474.2/79.9	57.7
CaNa-R3K2	861.4/30.5	2.5	943.0/69.9	42.2	1000.5/63.6	28.6	1054.7/66.8	25.1	1183.7/76.8	6.5	1412.5/76.5	45.3	1474.0/79.2	54.7
CaNa-R3K3	863.9/25.9	0.8	949.0/68.0	29.9	1018.5/65.3	37.7	1073.5/68.8	41.1	1186.7/66.5	2.8	1424.0/76.6	51.0	1480.5/79.9	49.0
CaNa-R3K4	864.1/24.6	0.3	951.4/70.7	21.9	1031.5/71.9	33.9	1084.4/68.0	43.9	1175.8/68.1	3.3	1427.8/75.5	50.4	1476.5/76.9	49.6
Ca-RnKp														
Ca-R2K1	872.6/31.1	2.2	929.4/71.8	39.2	987.4/71.8	22.3	1045.9/71.4	22.7	1212.7/74.8	5.2	1401.0/80.0	44.5	1468.1/81.0	55.5
Ca-R2K2	893.3/37.6	1.2	950.8/73.9	28.1	1028.6/75.1	30.1	1085.9/76.1	21.3	1183.6/89.8	5.5	1410.9/78.3	43.6	1468.2/78.4	56.4
Ca-R2K3	-	-	948.4/74.9	26.0	1029.1/75.0	36.6	1082.3/75.0	22.8	1177.9/87.0	8.0	1409.7/83.3	42.2	1466.6/83.7	57.8
Ca-R3K2	877.8/43.9	5.1	943.1/70.4	38.2	1009.7/68.5	23.6	1064.5/68.6	22.1	1195.2/92.1	6.0	1403.4/81.6	43.7	1468.6/83.8	56.3
Ca-R3K3	887.4/47.6	3.0	947.2/66.0	26.8	1023.0/72.8	25.4	1076.5/69.3	25.3	1169.2/94.1	7.2	1416.0/82.6	49.3	1471.1/85.0	50.7
Ca-R3K4			946.9/73.8	27.7	1023.7/73.6	30.6	1072.7/72.3	30.9	1168.2/88.4	7.5	1411.3/78.2	42.7	1464.6/85.0	57.3
CxNy														
C35N0	-	-	948.3/77.5	27.9	1022.5/79.1	47.0	1087.4/79.0	21.8	1223.4/87.1	3.4	1436.1/80.1	62.5	1495.6/82.9	37.5
C30N5	-	-	954.2/88.7	28.2	1021.5/81.8	43.3	1089.1/85.2	26.6	1183.4/73.0	1.9	1433.2/71.0	51.6	1483.6/70.1	48.4
C20N15	-	-	951.2/86.7	22.3	1022.6/90.4	46.7	1087.1/79.0	25.2	1184.2/118.4	5.8	1435.8/79.7	60.0	1491.8/76.4	40.0
C10N25	-	-	947.0/79.7	21.1	1011.0/77.9	34.2	1073.7/74.2	37.3	1157.7/87.5	7.3	1432.0/78.4	44.5	1484.5/73.7	55.5
C0N35	-	-	932.4/79.5	15.9	997.0/73.2	31.2	1068.4/71.1	44.9	1153.9/82.2	8.1	1435.4/78.1	43.9	1490.1/74.5	56.1
B15Nay														
B15Na10	-	-	948.4/99.3	8.6	1039.9/90.1	36.9	1107.9/65.7	27.5	1166.5/68.8	26.9	1397.6/92.1	50.0	1463.5/74.4	50.0
B15Na10	892.2/38.4	2.3	965.7/68.9	14.7	1044.0/71.0	32.6	1098.3/78.1	42.9	1167.7/71.6	7.5	1369.1/114.1	28.1	1472.3/86.9	71.9
B15Na30	864.8/25.8	0.3	961.4/90.1	23.7	1045.9/73.4	34.9	1088.9/65.6	36.9	1156.1/61.7	4.2	1407.6/97.1	26.1	1472.0/78.6	73.9
B15Na40	861.7/32.7	1.1	943.2/65.3	38.0	1004.4/54.9	20.7	1064.1/65.5	36.7	1165.3/62.5	3.5	1423.0/72.4	45.5	1478.3/73.9	54.5

Table S3. Previous XPS spectroscopic studies of silicate glasses and melts.

Literature	BO		NBO	
	B.E. (eV)	w. (eV)	B.E. (eV)	w. (eV)
D. Sprenger et al., 1990 [16]	532		530	
P. W. Wang et al., 1996 [17]	532		530	
A. Mekki et al., 1996 [18]	532		530	1.4
S. Matsumoto et al., 1998 [19]	531 –	1.5 –	529 –	1.4 –
	532	1.6	530	1.7
G. M. Bancroft et al., 2009 [20] (SiO ₂ glass)	533.2	1.25		
H. W. Nesbitt et al., 2011 [21]. 2015 [22]. 2017 [57,72]	531 –	1.2 –	529 –	1.2 –
	533	1.5	530	1.6
R. Sawyer et al., 2012 [25]. 2015 [26]	532 –	1.4 –	529 –	1.2 –
	533	1.5	530	1.5
J. Banerjee et al., 2016 [27]	532.5		531	
B. Roy et al., 2023 [28]	532	1.5	530	1.4

Table S4. Fit parameters deduced from XPS spectra: band energy (**B.E.**, ± 0.2 eV), full width at half maximum (**w.**, ± 0.1 eV) of band energy distribution and proportion of peak area (**%A**, ± 5 %).

Glass ID	O 1s XPS spectra deconvolution										Si 2p XPS spectra deconvolution		
	BO#1		BO#1		BO	NBO#1		NBO#2		NBO	Si 2p _{1/2}	Si 2p _{3/2}	w. (eV)
	B.E. (eV)	%A (%)	B.E. (eV)	%A (%)	w. (eV)	B.E. (eV)	%A (%)	B.E. (eV)	%A (%)	w. (eV)	B.E. (eV)	B.E. (eV)	
CaNa-RnKp													
CaNa-R2K1	533.5	5.1	531.8	52.4	1.8	531.2	40.8	529.6	1.7	1.4	102.1	102.7	1.5
CaNa-R2K2	533.4	5.3	531.8	62.6	1.8	531.1	27.9	530.0	4.2	1.5	102.1	102.7	1.6
CaNa-R2K3	533.9	3.0	532.1	74.4	1.8	531.2	16.7	530.1	5.9	1.5	102.4	103.0	1.6
CaNa-R3K2	533.4	7.2	532.0	47.4	1.7	531.2	39.6	530.2	5.8	1.5	102.2	102.8	1.6
CaNa-R3K3	533.5	4.0	532.2	54.1	1.7	531.3	35.4	530.2	6.6	1.5	102.4	103.0	1.6
CaNa-R3K4	533.5	25.2	532.0	49.1	1.6	531.5	18.1	530.3	7.6	1.6	101.9	102.5	1.5
Ca-RnKp													
Ca-R2K1	533.6	2.3	532.0	49.5	1.9	531.1	33.7	530.2	14.5	1.6	102.0	102.6	1.7
Ca-R2K2	534.2	2.2	532.4	50.4	1.7	531.5	33.7	530.4	13.7	1.7	102.5	103.1	1.8
Ca-R2K3	534.4	1.8	532.4	61.0	1.8	531.5	27.3	530.4	9.9	1.8	102.6	103.2	2.0
Ca-R3K2	-	-	532.5	25.9	1.9	531.6	45.1	530.5	29.0	1.7	102.2	102.8	1.9
Ca-R3K3	-	-	532.5	44.1	1.8	531.7	33.4	530.5	22.6	1.6	102.5	103.1	1.9
Ca-R3K4	-	-	532.6	97.0	1.8	-	-	530.2	3.0	1.6	103.2	103.8	1.7
CxNy													
C35N0	n.a.	n.a.	n.a.	n.a.	n.a.	n.a.	n.a.	n.a.	n.a.	n.a.	n.a.	n.a.	n.a.
C30N5	n.a.	n.a.	n.a.	n.a.	n.a.	n.a.	n.a.	n.a.	n.a.	n.a.	n.a.	n.a.	n.a.
C20N15	n.a.	n.a.	n.a.	n.a.	n.a.	n.a.	n.a.	n.a.	n.a.	n.a.	n.a.	n.a.	n.a.
C10N25	n.a.	n.a.	n.a.	n.a.	n.a.	n.a.	n.a.	n.a.	n.a.	n.a.	n.a.	n.a.	n.a.
C0N35	n.a.	n.a.	n.a.	n.a.	n.a.	n.a.	n.a.	n.a.	n.a.	n.a.	n.a.	n.a.	n.a.
B15Nay													
B15Na10	532.4	68.5	531.5	29.7	1.7	-	-	529.8	1.8	1.2	102.8	103.4	1.6
B15Na10	532.4	23.8	531.6	73.3	1.7	-	-	529.7	2.9	1.2	102.4	103.0	1.5
B15Na30	532.3	15.2	531.8	50.7	1.9	531.2	32.1	529.8	2.0	1.4	102.4	103.0	1.5
B15Na40	532.7	7.6	531.5	44.0	1.5	531.0	47.2	529.6	1.2	1.2	102.4	103.0	1.6

Table S5. Fit parameters deduced from EXAFS spectra in Ca-O shell: *k*-range (**k**), *R*-range (**R**), average distance between Ca and O atoms (**Avg. r_{Ca-O}**), Debye-Waller factor (**σ**), coordination number of neighboring O atoms of Ca (**CN_{Ca-O}**), average distance between Ca and Si atoms (**Avg. r_{Ca-Si}**) and coordination number of neighboring Si atoms of Ca (**CN_{Ca-Si}**). The error bars are reported in between brackets and were estimated from fit software.

Glass ID	Pre-edge (eV)	Edge (eV)	k (\AA^{-1})		R (\AA)		Ca-O#1		Ca-O#2		Ca-O#3		Avg. r_{Ca-O} (\AA)	CN _{Ca-O}	Avg. r_{Ca-Si} (\AA)	σ (\AA)	CN _{Ca-Si}
			min	max	min	max	r (\AA)	σ (\AA)	r (\AA)	σ (\AA)	r (\AA)	σ (\AA)					
CaNa-RnKp																	
CaNa-R2K1	4040.4	4043.6	3.0	10.0	1.15	3.15	2.85 (0.02)	0.015 (0.003)	2.50 (0.02)	0.022 (0.003)	2.30 (0.01)	0.011 (0.001)	2.55 (0.28)	5.8 (0.3)	3.40 (0.05)	0.018 (0.009)	1.9 (0.8)
CaNa-R2K2	4040.4	4043.6	3.0	10.0	1.15	3.15	2.95 (0.04)	0.029 (0.008)	2.73 (0.06)	0.035 (0.010)	2.31 (0.01)	0.009 (0.001)	2.66 (0.32)	5.8 (0.4)	3.44 (0.14)	0.023 (0.018)	1.8 (1.4)
CaNa-R2K3	4040.4	4043.6	3.0	10.0	1.15	3.15	2.95 (0.05)	0.026 (0.011)	2.75 (0.05)	0.027 (0.010)	2.32 (0.01)	0.010 (0.002)	2.67 (0.32)	6.4 (0.6)	3.42 (0.10)	0.010 (0.016)	1.5 (1.2)
CaNa-R3K2	4040.4	4043.6	3.0	10.0	1.15	3.15	2.84 (0.01)	0.011 (0.002)	2.51 (0.01)	0.014 (0.002)	2.28 (0.01)	0.009 (0.001)	2.54 (0.28)	5.7 (0.3)	3.39 (0.02)	0.011 (0.004)	2.6 (0.5)
CaNa-R3K3	4040.4	4043.6	3.0	10.0	1.15	3.15	2.89 (0.06)	0.017 (0.008)	2.61 (0.14)	0.041 (0.021)	2.31 (0.01)	0.012 (0.003)	2.60 (0.29)	5.7 (0.5)	3.45 (0.08)	0.016 (0.011)	2.5 (1.4)
CaNa-R3K4	4040.4	4043.6	3.0	10.0	1.15	3.15	2.88 (0.08)	0.034 (0.015)	2.79 (0.42)	0.059 (0.023)	2.31 (0.01)	0.010 (0.001)	2.66 (0.31)	6.0 (0.4)	3.41 (0.37)	0.041 (0.016)	3.8 (3.4)
Ca-RnKp																	
Ca-R2K1	4040.4	4043.6	3.0	10.0	1.15	3.15	2.87 (0.02)	0.019 (0.004)	2.57 (0.03)	0.028 (0.005)	2.32 (0.01)	0.012 (0.001)	2.59 (0.28)	5.9 (0.2)	3.42 (0.02)	0.011 (0.003)	2.1 (0.4)
Ca-R2K2	4040.4	4043.6	3.0	10.0	1.15	3.15	2.87 (0.01)	0.024 (0.002)	2.73 (0.10)	0.076 (0.022)	2.34 (0.01)	0.015 (0.001)	2.65 (0.27)	5.9 (0.2)	3.49 (0.04)	0.015 (0.006)	1.9 (0.4)
Ca-R2K3	4040.4	4043.6	3.0	10.0	1.15	3.15	2.87 (0.03)	0.029 (0.009)	2.82 (0.10)	0.056 (0.029)	2.34 (0.01)	0.014 (0.002)	2.68 (0.30)	6.0 (0.2)	3.51 (0.05)	0.016 (0.008)	2.0 (0.6)
Ca-R3K2	4040.4	4043.6	3.0	10.0	1.15	3.15	2.82 (0.02)	0.015 (0.003)	2.48 (0.02)	0.025 (0.004)	2.30 (0.01)	0.014 (0.001)	2.54 (0.26)	5.6 (0.3)	3.38 (0.03)	0.012 (0.005)	2.1 (0.6)
Ca-R3K3	4040.4	4043.6	3.0	10.0	1.15	3.15	2.86 (0.02)	0.015 (0.003)	2.54 (0.03)	0.036 (0.006)	2.31 (0.01)	0.016 (0.001)	2.57 (0.28)	5.7 (0.2)	3.45 (0.03)	0.009 (0.004)	2.0 (0.4)
Ca-R3K4	4040.5	4043.6	3.0	10.0	1.15	3.15	2.90 (0.02)	0.030 (0.004)	2.75 (0.03)	0.038 (0.006)	2.33 (0.01)	0.013 (0.001)	2.66 (0.30)	5.9 (0.2)	3.48 (0.04)	0.016 (0.007)	2.1 (0.5)

Table S6. ^{23}Na , ^{27}Al and ^{11}B NMR parameters deduced from the fits of 1D MAS-NMR spectra: isotropic chemical shift ($\delta_{\text{Na/Al/B}}$, ± 1.0 ppm), full width at half maximum (**FWHM**, ± 0.3 ppm) of isotropic chemical shift distribution, quadrupolar coupling constant ($\text{CQ}_{\text{Na/Al/B}}$, ± 0.2 MHz) and proportion (**Prop.**, ± 3 %). Czsimple and Amorphous are the models implemented in the dmfit program for (i.e. Na, Al and ^{11}B) and the G/L is the Gaussian/Lorentzian proportion of the peaks, where full Gaussian peak (G/L = 1) was used for fitting ^{11}B species.

Glass ID	^{23}Na NMR			^{27}Al (^{10}Al) NMR				^{11}B NMR														
	Czsimple			Czsimple				^{11}B I (Amorphous)				^{11}B II (Amorphous)				^{11}B 3Si (G/L)			^{11}B 4Si (G/L)			
	δ_{Na} (ppm)	FWHM (ppm)	CQ_{Na} (MHz)	$\delta_{[4]\text{Al}}$ (ppm)	FWHM (ppm)	$\text{CQ}_{[4]\text{Al}}$ (MHz)	Prop. (%)	δ_{B} (ppm)	FWHM (ppm)	CQ_{B} (MHz)	Prop. (%)	δ_{B} (ppm)	FWHM (ppm)	CQ_{B} (MHz)	Prop. (%)	δ_{B} (ppm)	FWHM (ppm)	Prop. (%)	δ_{B} (ppm)	FWHM (ppm)	Prop. (%)	
CaNa-RnKp																						
CaNa-R2K1	6.5	20.4	3.2	67.3	11.1	5.0	100.0	19.5	3.4	2.6	59.4	15.5	4.0	2.3	23.7	0.7	2.5	16.9				
CaNa-R2K2	1.0	19.8	3.2	64.8	11.8	5.1	100.0	18.5	3.4	2.5	41.9	14.4	4.0	2.3	17.4	0.4	2.6	33.4	-0.9	2.0	7.2	
CaNa-R2K3	-3.2	20.3	3.0	63.0	11.3	5.3	100.0	17.8	3.4	2.5	35.6	13.5	4.0	2.3	12.1	-0.3	2.7	47.2	-1.6	2.0	5.1	
CaNa-R3K2	6.0	20.1	3.3	66.7	11.0	4.9	100.0	19.2	3.4	2.5	52.2	15.2	4.0	2.3	25.4	0.5	2.7	22.4				
CaNa-R3K3	2.6	20.5	3.3	65.2	11.7	5.1	100.0	18.4	3.4	2.5	45.3	14.4	4.0	2.3	16.0	0.1	2.4	32.5	-1.2	1.9	6.2	
CaNa-R3K4	-0.5	20.4	3.2	63.7	11.0	5.1	100.0	17.8	3.4	2.5	37.5	13.9	4.0	2.3	11.6	-0.2	2.7	44.4	-1.6	2.0	6.6	
Ca-RnKp																						
Ca-R2K1	-	-	-	66.3	13.5	6.6	80.9	18.8	4.0	2.6	53.1	15.5	5.0	2.5	25.8	0.4	2.9	21.1				
Ca-R2K2	-	-	-	63.4	14.0	6.9	89.2	18.1	4.0	2.6	38.9	15.0	5.0	2.6	34.4	-0.1	2.8	23.7	-1.4	2.4	3.1	
Ca-R2K3	-	-	-	62.7	14.0	6.9	90.0	18.2	4.0	2.6	34.6	14.4	5.0	2.6	41.1	0.0	2.7	18.4	-1.4	2.4	6.0	
Ca-R3K2	-	-	-	65.9	13.5	6.6	83.4	18.8	4.0	2.6	44.6	15.4	5.0	2.5	31.5	0.0	2.8	23.9				
Ca-R3K3	-	-	-	63.9	14.0	6.8	89.6	18.2	4.0	2.6	40.0	14.7	5.0	2.5	34.1	-0.2	2.8	22.4	-1.4	2.4	3.5	
Ca-R3K4	-	-	-	63.1	13.0	6.8	89.4	18.2	4.0	2.6	39.0	5.0	5.0	2.5	37.5	-0.1	2.7	16.6	-1.4	2.4	6.9	
CxNy																						
C35N0	-	-	-	62.8	-	6.1		18.3	4.0	2.6	48.7	14.6	5.0	2.5	18.6	0.8	2.9	21.8	-0.4	2.7	10.9	
C30N5	-7.7	-	2.6	62.9	-	5.7		18.3	4.0	2.6	47.4	14.7	5.0	2.5	17.3	1.0	2.9	22.2	-0.4	2.7	13.1	
C20N15	-3.6	-	2.9	63.9	-	4.9		18.2	4.0	2.5	48.9	13.8	5.0	2.4	10.5	0.8	2.9	29.1	-0.4	2.7	11.5	
C10N25	-0.6	-	3.1	64.6	-	4.8		18.9	3.0	2.5	36.3	15.6	5.0	2.4	19.5	0.7	2.9	39.2	-0.4	2.7	5.0	
C0N35	1.3	-	3.2	64.9	-	4.6		18.9	3.0	2.5	40.8	14.5	5.0	2.4	12.4	0.8	2.9	46.2	-0.4	2.7	0.7	
BxNy																						
B15Na10	-12.4	18.6	2.5	59.2	12.2	5.1	100.0	17.1	4.5	2.7	37.2	13.4	4.0	2.6	27.1	-0.6	2.4	25.9	-2.2	1.8	9.8	
B15Na10	-6.5	22.2	2.8	61.8	11.4	5.2	100.0	17.1	4.0	2.5	27.9	12.6	4.0	2.6	7.4	-0.6	2.7	51.4	-2.0	1.8	13.3	
B15Na30	-0.5	23.0	2.9	63.7	10.4	5.0	100.0	18.3	2.9	2.6	27.5	14.3	3.0	2.2	11.2	0.0	2.7	52.3	-1.3	2.2	9.0	
B15Na40	3.4	22.4	2.7	65.8	10.7	4.5	100.0	18.5	4.0	2.4	42.6	14.0	4.0	2.3	20.5	0.6	2.4	32.7	-0.6	1.8	4.2	

Table S7. ^{11}B NMR parameters of CaNa-R2K1 and B15Na10 glasses deduced from the ^{11}B DQ-SQ SQ projections, ^{11}B SE spectra and ^{11}B MAS-NMR spectra decomposition: chemical shift (δ_{B} , ± 0.3 ppm), full width at half maximum (**FWHM**, ± 0.3 ppm) of chemical shift distribution and proportion (**Prop.**, ± 3 %).

NMR techniques	$^{[4]}\text{B}(3\text{Si},1\text{B})$			$^{[4]}\text{B}(4\text{Si},0\text{B})$		
	δ_{B} (ppm)	FWHM (ppm)	Prop. (%)	δ_{B} (ppm)	FWHM (ppm)	Prop. (%)
CaNa-R2K1						
DQ proj.	0.9	2.4	100			
SE (75 ms)	0.6	2.4	100			
SE (25 ms)	0.6	2.3	100			
SE (0.05 ms)	0.7	2.7	100			
MAS-NMR	0.7	2.5	100			
B15Na10						
DQ proj.	-0.4	2.4	100			
SE (75 ms)	-0.8	2.4	48.5	-2.5	1.8	51.5
SE (25 ms)	-0.7	2.4	55.2	-2.4	1.8	44.8
SE (0.05 ms)	-0.5	2.6	76.7	-2.2	1.8	23.3
MAS-NMR	-0.6	2.4	72.5	-2.2	1.8	27.5

Table S8. ^{11}B NMR parameters of CaNa-RnKp glass series deduced from the ^{11}B DQ-SQ DQ projections decomposition: chemical shift (δ_{B} , ± 0.3 ppm), full width at half maximum (**FWHM**, ± 0.3 ppm) of chemical shift distribution and proportion (**Prop.**, ± 3 %).

Glass ID	$^{[3]}\text{B-O-}^{[3]}\text{B}_I$			$^{[3]}\text{B-O-}^{[3]}\text{B}_{II}$			$^{[3]}\text{B-O-}^{[4]}\text{B}_I$			$^{[3]}\text{B-O-}^{[4]}\text{B}_{II}$		
	δ_{B} (ppm)	FWHM (ppm)	Prop. (%)	δ_{B} (ppm)	FWHM (ppm)	Prop. (%)	δ_{B} (ppm)	FWHM (ppm)	Prop. (%)	δ_{B} (ppm)	FWHM (ppm)	Prop. (%)
CaNa-R2K1	29.0	8.0	42.5	22.3	8.9	41.5	15.1	3.8	5.4	11.5	5.9	10.9
CaNa-R2K2	28.5	6.8	30.0	21.5	8.5	34.0	14.7	4.3	14.7	10.4	6.5	22.4
CaNa-R2K3	27.6	6.7	23.6	20.8	8.6	28.1	14.2	4.1	22.0	9.1	5.8	26.3
CaNa-R3K2	29.1	7.5	39.0	22.1	8.5	42.4	15.4	3.4	6.0	11.1	5.8	12.6
CaNa-R3K3	27.8	6.8	27.5	21.5	8.5	36.1	14.7	3.4	14.5	10.4	5.8	22.0
CaNa-R3K4	27.8	6.8	23.6	21.3	8.5	29.9	14.2	3.4	18.0	10.1	5.8	28.6

Reference (Suppl. Mat.)

- (1) Mysen, B. O.; Virgo, D.; Scarfe, C. M. Relations between the Anionic Structure and Viscosity of Silicate Melts—a Raman Spectroscopic Study. *Am. Mineral.* **1980**, *65* (7–8), 690–710.
- (2) Mysen, B. O.; Virgo, D.; Seifert, F. A. The Structure of Silicate Melts: Implications for Chemical and Physical Properties of Natural Magma. *Rev. Geophys.* **1982**, *20* (3), 353–383. <https://doi.org/10.1029/RG020i003p00353>.
- (3) Matson, D. W.; Sharma, S. K.; Philpotts, J. A. The Structure of High-Silica Alkali-Silicate Glasses. A Raman Spectroscopic Investigation. *J. Non-Cryst. Solids* **1983**, *58* (2–3), 323–352. [https://doi.org/10.1016/0022-3093\(83\)90032-7](https://doi.org/10.1016/0022-3093(83)90032-7).
- (4) McMillan, P. Structural Studies of Silicate Glasses and Melts—Applications and Limitations of Raman Spectroscopy. *Am. Mineral.* **1984**, *69* (7–8), 622–644.
- (5) Frantz, J. D.; Mysen, B. O. Raman Spectra and Structure of BaO-SiO₂ SrO-SiO₂ and CaO-SiO₂ Melts to 1600°C. *Chem. Geol.* **1995**, *121* (1–4), 155–176. [https://doi.org/10.1016/0009-2541\(94\)00127-T](https://doi.org/10.1016/0009-2541(94)00127-T).
- (6) Akagi, R.; Ohtori, N.; Umesaki, N. Raman Spectra of K₂O–B₂O₃ Glasses and Melts. *J. Non-Cryst. Solids* **2001**, *293–295*, 471–476. [https://doi.org/10.1016/S0022-3093\(01\)00752-9](https://doi.org/10.1016/S0022-3093(01)00752-9).
- (7) Cormier, L.; Majérus, O.; Neuville, D. R.; Calas, G. Temperature-Induced Structural Modifications Between Alkali Borate Glasses and Melts. *J. Am. Ceram. Soc.* **2006**, *89* (1), 13–19. <https://doi.org/10.1111/j.1551-2916.2005.00657.x>.
- (8) Zakaznova-Herzog, V. P.; Malfait, W. J.; Herzog, F.; Halter, W. E. Quantitative Raman Spectroscopy: Principles and Application to Potassium Silicate Glasses. *J. Non-Cryst. Solids* **2007**, *353* (44–46), 4015–4028. <https://doi.org/10.1016/j.jnoncrysol.2007.06.033>.
- (9) Lenoir, M.; Grandjean, A.; Linard, Y.; Cochain, B.; Neuville, D. R. The Influence of Si,B Substitution and of the Nature of Network-Modifying Cations on the Properties and Structure of Borosilicate Glasses and Melts. *Chem. Geol.* **2008**, *256* (3–4), 316–325. <https://doi.org/10.1016/j.chemgeo.2008.07.002>.
- (10) Manara, D.; Grandjean, A.; Neuville, D. R. Advances in Understanding the Structure of Borosilicate Glasses: A Raman Spectroscopy Study. *Am. Mineral.* **2009**, *94* (5–6), 777–784. <https://doi.org/10.2138/am.2009.3027>.
- (11) Angeli, F.; Villain, O.; Schuller, S.; Charpentier, T.; De Ligny, D.; Bressel, L.; Wondraczek, L. Effect of Temperature and Thermal History on Borosilicate Glass Structure. *Phys. Rev. B* **2012**, *85* (5), 054110. <https://doi.org/10.1103/PhysRevB.85.054110>.
- (12) Neuville, D. R.; De Ligny, D.; Henderson, G. S. Advances in Raman Spectroscopy Applied to Earth and Material Sciences. *Rev. Mineral. Geochem.* **2014**, *78* (1), 509–541. <https://doi.org/10.2138/rmg.2013.78.13>.
- (13) Le Losq, C.; Neuville, D. R.; Florian, P.; Henderson, G. S.; Massiot, D. The Role of Al³⁺ on Rheology and Structural Changes in Sodium Silicate and Aluminosilicate Glasses and Melts. *Geochim. Cosmochim. Acta* **2014**, *126*, 495–517. <https://doi.org/10.1016/j.gca.2013.11.010>.
- (14) Moulton, B. J. A.; Silva, L. D.; Doerenkamp, C.; Lozano, H.; Zanutto, E. D.; Eckert, H.; Pizani, P. S. Speciation and Polymerization in a Barium Silicate Glass: Evidence from ²⁹Si NMR and Raman Spectroscopies. *Chem. Geol.* **2021**, *586*, 120611. <https://doi.org/10.1016/j.chemgeo.2021.120611>.
- (15) Nesbitt, H. W.; Henderson, G. S.; Bancroft, G. M.; Neuville, D. R. Spectral Resolution and Raman Q³ and Q² Cross Sections in ~40 Mol% Na₂O Glasses. *Chem. Geol.* **2021**, *562*, 120040. <https://doi.org/10.1016/j.chemgeo.2020.120040>.
- (16) Sprenger, D.; Bach, H.; Meisel, W.; Gülich, P. XPS Study of Leached Glass Surfaces. *J. Non-Cryst. Solids* **1990**, *126* (1–2), 111–129. [https://doi.org/10.1016/0022-3093\(90\)91029-Q](https://doi.org/10.1016/0022-3093(90)91029-Q).
- (17) Wang, P. W.; Zhang, L. Structural Role of Lead in Lead Silicate Glasses Derived from XPS Spectra. *J. Non-Cryst. Solids* **1996**, *194* (1–2), 129–134. [https://doi.org/10.1016/0022-3093\(95\)00471-8](https://doi.org/10.1016/0022-3093(95)00471-8).

- (18) Mekki, A.; Holland, D.; McConville, C. F.; Salim, M. An XPS Study of Iron Sodium Silicate Glass Surfaces. *J. Non-Cryst. Solids* **1996**, *208* (3), 267–276. [https://doi.org/10.1016/S0022-3093\(96\)00523-6](https://doi.org/10.1016/S0022-3093(96)00523-6).
- (19) Matsumoto, S.; Nanba, T.; Miura, Y. X-Ray Photoelectron Spectroscopy of Alkali Silicate Glasses. *J. Ceram. Soc. Jpn.* **1998**, *106* (1232), 415–421. <https://doi.org/10.2109/jcersj.106.415>.
- (20) Bancroft, G. M.; Nesbitt, H. W.; Ho, R.; Shaw, D. M.; Tse, J. S.; Biesinger, M. C. Toward a Comprehensive Understanding of Solid-State Core-Level XPS Linewidths: Experimental and Theoretical Studies on the Si 2p and O 1s Linewidths in Silicates. *Phys Rev B* **2009**, *80* (7), 075405. <https://doi.org/10.1103/PhysRevB.80.075405>.
- (21) Nesbitt, H. W.; Bancroft, G. M.; Henderson, G. S.; Ho, R.; Dalby, K. N.; Huang, Y.; Yan, Z. Bridging, Non-Bridging and Free (O^{2-}) Oxygen in Na_2O-SiO_2 Glasses: An X-Ray Photoelectron Spectroscopic (XPS) and Nuclear Magnetic Resonance (NMR) Study. *J. Non-Cryst. Solids* **2011**, *357* (1), 170–180. <https://doi.org/10.1016/j.jnoncrysol.2010.09.031>.
- (22) Nesbitt, H. W.; Bancroft, G. M.; Henderson, G. S.; Sawyer, R.; Secco, R. A. Direct and Indirect Evidence for Free Oxygen (O^{2-}) in MO-Silicate Glasses and Melts (M = Mg, Ca, Pb). *Am. Mineral.* **2015**, *100* (11–12), 2566–2578. <https://doi.org/10.2138/am-2015-5336>.
- (23) Nesbitt, H. W.; Bancroft, G. M.; Ho, R. XPS Valence Band Study of Na-Silicate Glasses: Energetics and Reactivity. *Surf. Interface Anal.* **2017**, *49* (13), 1298–1308. <https://doi.org/10.1002/sia.6262>.
- (24) Nesbitt, H. W.; Henderson, G. S.; Bancroft, G. M.; O’Shaughnessy, C. Electron Densities over Si and O Atoms of Tetrahedra and Their Impact on Raman Stretching Frequencies and Si-NBO Force Constants. *Chem. Geol.* **2017**, *461*, 65–74. <https://doi.org/10.1016/j.chemgeo.2016.11.022>.
- (25) Sawyer, R.; Nesbitt, H. W.; Secco, R. A. High Resolution X-Ray Photoelectron Spectroscopy (XPS) Study of K_2O-SiO_2 Glasses: Evidence for Three Types of O and at Least Two Types of Si. *J. Non-Cryst. Solids* **2012**, *358* (2), 290–302. <https://doi.org/10.1016/j.jnoncrysol.2011.09.027>.
- (26) Sawyer, R.; Nesbitt, H. W.; Bancroft, G. M.; Thibault, Y.; Secco, R. A. Spectroscopic Studies of Oxygen Speciation in Potassium Silicate Glasses and Melts. *Can. J. Chem.* **2015**, *93* (1), 60–73. <https://doi.org/10.1139/cjc-2014-0248>.
- (27) Banerjee, J.; Kim, S. H.; Pantano, C. G. Elemental Areal Density Calculation and Oxygen Speciation for Flat Glass Surfaces Using X-Ray Photoelectron Spectroscopy. *J. Non-Cryst. Solids* **2016**, *450*, 185–193. <https://doi.org/10.1016/j.jnoncrysol.2016.07.029>.
- (28) Roy, B.; Baier, F.; Rosin, A.; Gerdes, T.; Schafföner, S. Structural Characterization of the Near-Surface Region of Soda–Lime–Silica Glass by X-Ray Photoelectron Spectroscopy. *Int. J. Appl. Glass Sci.* **2023**, *14* (2), 229–239. <https://doi.org/10.1111/ijag.16604>.